Cheng, Qiang; Hulkkonen, Tuomo; Kaario, Ossi; Larmi, Martti

Spray dynamics of HVO and EN590 diesel fuels

Published in:
Fuel

DOI:
10.1016/j.fuel.2019.01.123

Published: 01/06/2019

Document Version
Peer-reviewed accepted author manuscript, also known as Final accepted manuscript or Post-print

Please cite the original version:
Cheng, Q., Hulkkonen, T., Kaario, O., & Larmi, M. (2019). Spray dynamics of HVO and EN590 diesel fuels. *Fuel*, *245*, 198-211. https://doi.org/10.1016/j.fuel.2019.01.123

Spray Dynamics of HVO and EN590 Diesel Fuels

Qiang Cheng[a], Hulkkonen Tuomo[b], Ossi Tapani Kaario[a], Larmi Martti[a]

[a] ***Aalto University, School of Engineering, Department of Mechanical Engineering, 00076 Aalto, Finland***

[b] ***Energy Authority, FIN-00530 Helsinki, Finland***

Abstract: This investigation aims at quantifying the spray dynamics of diesel-like injection at the steady stage. A 1D model based on momentum flux conservation and combined with Gaussian radial profiles is derived to predict the axial and radial velocity, fuel concentration, liquid volume fraction and density distribution within the steady spray field. To validate the model over a range of conditions, global quantities such as spray tip penetration, spray cone angle, spray tip velocity, and spray volume was measured by diffused back-illumination imaging. The spray characteristics of hydrotreated vegetable oil (HVO) and European standard diesel fuel (EN590) under different ambient air conditions (36kg/m^3 and 115kg/m^3) are compared to further predict the local velocity, fuel concentration, liquid volume fraction and density distribution. The present results indicate that an accurate model of diesel-like spray evolution can be obtained for different fuel types and ambient air densities.

Keywords: Diffused back-illumination Imaging, Diesel Spray, 1D model, HVO and EN590

Introduction

The common rail injection system, which has been developed to improve the spray quality and injection strategies, is capable of increasing engine efficiency and decreasing emissions. Researchers in the field have focused on atomization, air entrainment, mixing and evaporation of diesel spray [1,2]. However, the detailed mechanism of fuel spray formation and fuel-air entrainment is still scalcely understood, calling for an in-depth understanding of the dynamic behavior of the diesel-like spray.

To explain the underlying physics, several optical approaches have been taken to visualize the macroscopic and microscopic characteristics of the spray. The most typical parameters include spray tip penetration and spray cone angle, which are macroscopic characteristics that can be obtained by Mie scattering, shadowgraphy, diffused back-illumination and high-speed schlieren imaging. However, except for the morphology information for the above techniques that can be provided, the quantitative data that can be measured is minimal. To obtain more local flow field information, such as velocity, fuel concentration, and density distribution, more complicated and expensive optical diagnostics techniques have to be established to satisfy the measuring requirements. For the local velocity measurement, particle image velocimetry (PIV) is most typically adopted for flow field measurement. However, it is difficult generally to measure the dense area of the spray near the nozzle[3]. Planar laser-induced fluorescence (PLIF) or planar laser induced fluorescence (PLIEF) can provide relatively strong signals from the vapor and the liquid phases to measure the fuel concentration or mass fraction from the liquid spray. However, oxygen quenches the fluorescence from many tracer species [4].

Additionally, PLIF or PLIEF requires complex optics, high-powered lasers and fuel additives[5]. Only a few studies focus on the quantitative spray density measurement. A recent example can be found in [6], which implemented the background-oriented schlieren (BOS) technique to visualize the difference in the temporary change in the density distribution by solving Poisson's equation. This method can be applied to obtain full-scale visualization of the density fields with a promising spatial resolution. However, the alignment of the optical circuit is complicated, and the precision of the results is highly dependent on the optical parameters.

With the development of computer science and Computational Fluid Dynamics (CFD), more details of the spray structures can be simulated with 2D or 3D models. However, the complicacies of the model validation and the balance between the computational costs and the accuracy of the results may still be prohibitive. For example, Reynolds Averaged Navier–Stokes (RANS) is commonly used in CFD to perform 3D simulations [7, 8], characterized by reasonable computational costs. However, it allows the no origins, e.g., cyclic variabilities [9]. Large Eddy Simulation (LES) seems to be better adapted to such situations[10]. However, in principle, LES reduces the computational cost by removing small-scale information from the numerical solution. Since this information is not irrelevant, it has to be carefully modeled, otherwise, the accuracy of the simulation results could be questioned. The Direct Numerical Simulation (DNS) can be used to solve the turbulence flow in an extensive range of time and length scales without any turbulence model. Nevertheless, DNS is computationally expensive, and its cost prohibits simulation of practical engineering systems with complex geometry or flow configurations [11].

A simplified model represents a low computational cost, high efficiency and reasonable predictions on spray dynamic properties and evolutions. Recently, 1D models are commonly applied to spray penetration and spray cone angle predictions [12]. Many advances have been made in the fluid mechanics of single jets, and quantitative and qualitative bases established for the jet theory can be conveniently adopted for the diesel spray [13]. Several studies have considered momentum flux as the vital parameter to govern the spray dynamics [14-16]. Before conducting the momentum flux for the spray flow field simulation, the behavior of the liquid flow inside the injector nozzle has to be adequately measured or estimated, as it has a significant effect on the spray behavior. For example, cavitation may occur depending on the nozzle geometry and flow properties [17]. Furthermore, the velocity at the nozzle exit is critical for estimating the initial momentum, as it will be needed to derive the spray penetration, cone angle, and velocity. Since the primary break-up is challenging to observe experimentally, the downstream of the nozzle distance for the primary break-up should be calculated appropriately. Ueki et al. [18] concluded that the jet disintegration was complete at the 7.5D exit. Once the initial velocity and spray cone angle are obtained, the spray penetration and velocity can be calculated by the mass and momentum conservation theory. Siebers [19] developed a scaling law for the maximum penetration distance of liquid phase fuel in a diesel spray based on jet theory. The comparison of the scaling covered a wide range of conditions, and a close agreement was shown between the liquid length scaling law and the measured data. After the 1D model validation, an additional feature concerning the radial evolution of axial velocity and fuel concentration assuming fully developed conditions [20-22]. It is notable that the 1D model has to be validated by experimental data. However, it is independent of the experiments. Once the accuracy of the model has been proven, it can be conducted to predict the spray characteristics independently. However, present information of these kinds of models is limited, because there is a straightforward identification of the link between the outer edge conditions and the results[23]. The present work performs direct visualization of atomizing sprays with diffused back-illumination imaging combined with the 1D model to obtain both qualitative and quantitative information on spray fields.

This paper reports an investigation that aims at combining a 1D model with diffused back-illumination imaging techniques to analyze the relationship among the spray momentum flux, fuel-air mixing and dynamic evolution. The 1D model based on momentum flux conservation along the spray axis is validated with the experimental data. It then presents a mathematical model which relates the momentum flux with axial profiles of velocity, fuel concentration, liquid volume fraction and spray density. Finally, the 1D model combined with the spray outer edge measured by means of diffused back-illumination imaging was employed to calculate the spray field characteristics pixel-by-pixel. The main contribution of the present study, which makes it different from previous investigations, is the combination of a 1D model and simple imaging techniques for spray field estimation.

The current investigation can be divided into five sections. In Section 2, the velocity of the liquid jet at the nozzle exit is determined and calculated based on the model from Sarre et al. [24]. Further, the mass and momentum conservation theory was adopted to derive the velocity at the axis. In Section 3, the Gaussian radial profile is assumed for velocity along the spray tip direction, then the local velocity, fuel concentration, and density distribution are calculated based on the Gaussian radial profile. In Section 4, the numerical model was validated against experimental data. In Section 5, the spray characteristics of the HVO and EN590 under different conditions are performed and compared.

Nomenclature			
A	ambient air mass flow rate	P_{vena}	the pressure at vena-contracta
A_{eff}	effective nozzle area	S_{tip}	spray tip penetration
A_{exit}	nozzle exit area	S_c	the Schmidt number
B	spray cone angle coefficient	t	time
$C(z,r)$	the local fuel concentration	$U(z,r)$	the velocity along the z direction
$C_{axis}(z))$	fuel concentration in the coordinate z of the spray center axis	$U_{axis}(z)$	velocity in the coordinate z of the spray center axis
C_c	contraction coefficient	U_{exit}	the velocity at nozzle exit
C_d	the discharge coefficient	U_{mean}	mean velocity at nozzle exit
D	nozzle diameter	$U_{rad}(z)$	the velocity at radial direction
f	Blasius or the laminar equation for wall friction	U_{tip}	average spray tip velocity
F	fuel mass flow rate	U_{vena}	the velocity at vena-contracta
k	velocity coefficient in the spray model	Z,Y_f	mixture fraction
K_{inlet}	inlet loss coefficients	Greek symbols	
L	nozzle length	α	coefficient of the Gaussian radial profile for theaxial velocity
P_{amb}	Ambient air pressure	ρ_a	Ambient air density
m	exponential coefficient of spray cone angle model	ρ_f	Fuel density
$\dot{M}(z)$	momentum in the coordinate z of the spray center axis	$\rho(z,r)$	the local density at the position (z,r)
$\dot{M}_{exit}$	momentum at nozzle exit	ω	non-dimensional radial coordinate ($\omega = r/R$)
P_{inj}	Fuel injection Pressure	θ	spray cone angle
P_{vap}	saturation vapor pressure of the fuel	$\bar{\chi}$	Liquid volume fraction

2. Numerical model derivation

2.1 Velocity at the nozzle Exit

The initial spray conditions are highly dependent on the flow inside the nozzle. As a consequence, the flow conditions inside the nozzle need to be determined first [14, 24]. The velocity of the liquid jet at the nozzle exit, U_{exit}, depends on whether the flow inside the nozzle is cavitating or merely turbulent [24]. To better visualize the flow condition inside the injector nozzle, Fig.1 demonstrates the atomization processes of diesel-like fuel injected from a nozzle.

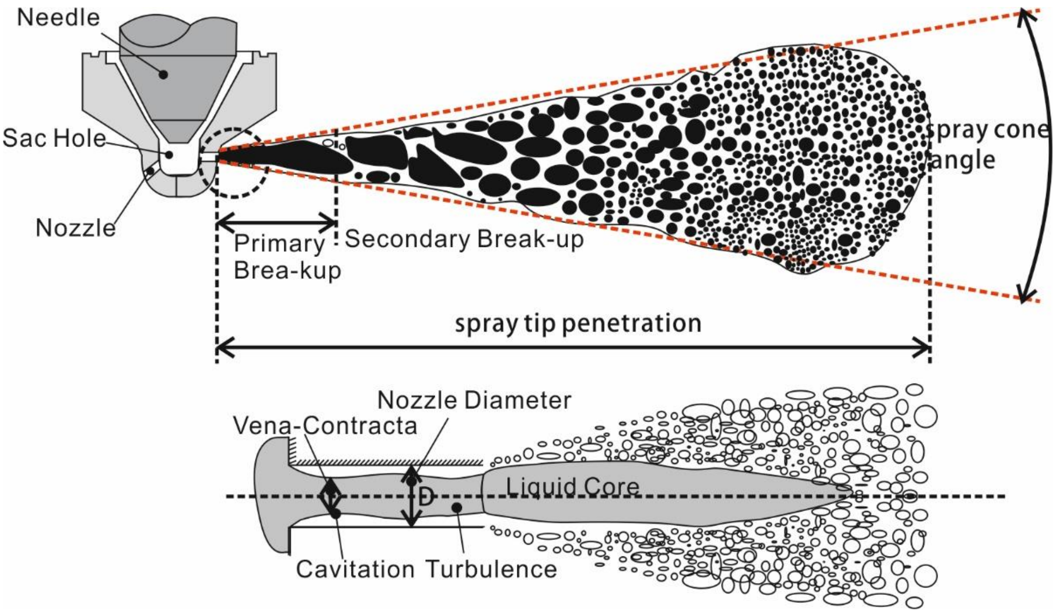

Fig.1 Flow conditions inside the nozzle and spray characteristics outside at the nozzle exit

Despite the fact that fluid velocity at the nozzle exit can be calculated from typical Bernoulli principle, the mean velocity of the flow is always lower than the theoretical value due to the losses. To obtain an accurate U_{exit}, the discharge coefficient C_d is considered to quantify the difference.

$$U_{mean} = C_d \sqrt{\frac{2 \cdot (P_{inj} - P_{amb})}{\rho_f}} \tag{1}$$

In case of a turbulent flow, the tabulated inlet loss coefficients K_{inlet} and the Blasius or the laminar equation for wall friction are applied to discharge coefficient C_d derivation [25].

$$C_d = \frac{1}{\sqrt{K_{inlet} + f \cdot \frac{L}{D} + 1}} \tag{2}$$

Where f is the Blasius or the laminar equation for wall friction: $f = Max(0.316 \cdot Re^{-0.25}, 64/Re)$

In case of a cavitating flow, the Nurick's expression [26, 27] for the size of contraction can be utilized to estimate the velocity at the smallest flow area.

$$U_{vena} = \frac{U_{mean}}{C_c} \tag{3}$$

$$C_c = \left(\frac{\pi+2}{\pi}\right)^2 - 11.4 \cdot \frac{r}{D} \tag{4}$$

$$P_{vena} = P_{inj} - \frac{\rho f}{2} \cdot U_{vena}^2 = P_{inj} - \frac{\rho f}{2} \cdot \left(\frac{U_{mean}}{C_c}\right)^2 \tag{5}$$

If $P_{vena} > P_{vapor}$, the flow inside the nozzle is a no-cavitating flow. The fuel injection pressure is assumed as the effective pressure, and the effective area is the geometrical area of the nozzle cross section.

$$U_{exit} = U_{mean} = C_d \sqrt{\frac{2 \cdot (P_{inj} - P_{amb})}{\rho_f}} \tag{6}$$

If $P_{vena} < P_{vapor}$, it is assumed that the flow must be fully cavitating, and a new inlet pressure and effective area have to be estimated. A new discharge coefficient can be estimated as:

$$C_d = C_c \sqrt{\frac{P_{inj} - P_{vap}}{P_{inj} - P_{amb}}} \tag{7}$$

The velocity in the vena-contracta becomes:

$$U_{vena} = \sqrt{\frac{2 \cdot (P_{inj} - P_{vap})}{\rho_f}} \tag{8}$$

By application of the mass and momentum conversation equations, the velocity at the nozzle exit can be obtained [27]:

$$U_{exit} = U_{vena} - \frac{P_{amb} - P_{vap}}{\rho_f \cdot U_{mean}} \tag{9}$$

$$A_{eff} = A_{exit} \frac{U_{mean}}{U_{exit}} \tag{10}$$

2.2 Momentum Flux

Before the application of the momentum conservation equation for diesel-like spray momentum flux, the hypotheses assumed to perform the theoretical derivation of the model are given [13, 15, 23]:

(1) The environment in the spray chamber is quiescent.
(2) The spray velocity along the x-direction obeys the Gaussian radial profile.
(3) Momentum, injection velocity and mass flow rate are constant during the entire injection process.
(4) Ambient air pressure and density keep steady, even the fuel injected into the spray chamber.
(5) The spray is in no-evaporation condition.

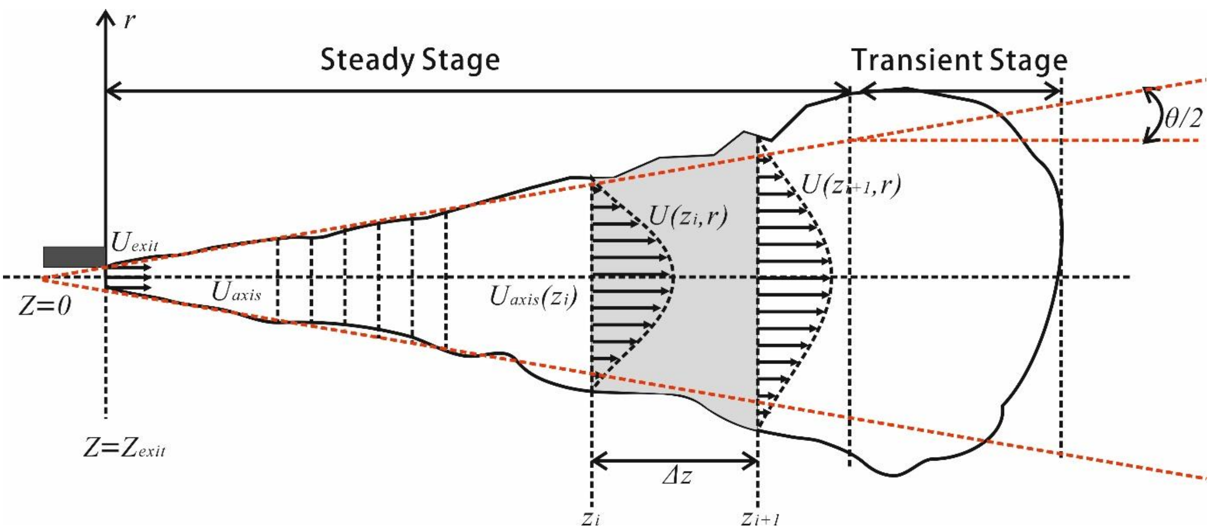

Fig. 2. Schematic of the model approach.

The schematic in Fig.2 shows a coordinates system *(z,r)* which can describe the basic configuration of this type of problem. A similar description can also be seen in [13, 27]. The momentum flux at distance *z* plane can be written as:

$$\dot{M}(z) = \dot{M}_{exit} = \int_0^R 2\pi\rho(z,r) r U^2(z,r) dr \tag{11}$$

where $\dot{M}_{exit} = \rho_f \cdot A_{eff} \cdot U_{exit}^2$, $\rho(z,r)$ is the local density at the position *(z,r)*, and $U(z,r)$ is the velocity along the z direction defined by Gaussian radial profiles:

$$U(z,r) = U_{axis}(z) e^{-\alpha\omega^2} \tag{12}$$

where $U_{axis}(z)$ is the velocity at the center axis of the spray, r is the radial position, R is the outer edge radius of the half spray width, α is a shape factor of the Gaussian distribution[15, 28], and $\omega = \frac{r}{R}$.

By solving the Eq. (11), the $U_{axis}(z)$ can be obtained:

$$U_{axis}(z) = \frac{\dot{M}_{exit}^2}{\left[\rho_a \cdot \frac{\pi}{2\alpha} \cdot (1-e^{-2\alpha})\right]^{\frac{1}{2}} \cdot z \cdot tan^2\left(\frac{\theta}{2}\right)} \tag{13}$$

$$U_{rad}(z) = U_{axis}(z) \cdot tan\left(\frac{\theta}{2}\right) \cdot \omega \tag{14}$$

It is obviously found that the velocity along the axis is relevant to the tip penetration velocity. Assuming that the velocity along the axis is proportional to the tip penetration velocity, the relationship between these two parameters can be written as:

$$U_{axis}\left(z = S_{tip}\right) = k \cdot U_{tip} = k \cdot \frac{dS_{tip}}{dt} \tag{15}$$

By solving the Eq. (15), the spray tip penetration can be estimated as:

$$S_{tip} = \frac{2}{k} \cdot \left(\frac{2\alpha}{\pi} \cdot t^2\right)^{\frac{1}{4}} \cdot \left[\frac{\dot{M}_{exit}}{\rho_a \cdot (1-e^{-2\alpha}) \cdot tan^2\left(\frac{\theta}{2}\right)}\right]^{\frac{1}{4}} \tag{16}$$

In the above formula, k is a constant value that can be correlated by means of the measurements, and the k is 2.076 after calibration. α can be estimated on the assumption that the radial position r=R and $U(z,r)$=0.01U_{axis}, a value of $\alpha = 4.605$ can be obtained.

According to Eq. (13), the spray cone angle has to be predicted before calculating. Based on the empirical formula derived by Reitz and Bracco [29], the spray cone angle can be written as:

$$\theta = \frac{360}{\pi} \arctan\left(B\left(\frac{\rho_a}{\rho_l}\right)^m\right) \tag{17}$$

where B and m are the empirical coefficients. Reitz and Bracco obtained these values: B=0.4275, m=0.5. However, as the study of Reitz and Bracco [29] was based on a lower pressure system rather than a modern common rail injection system, it does not fit to the present experimental plots. After the model validation, the coefficient of Eq. (17) is changed to B=0.31, m=0.25.

2.3 Gaussian Radial Distribution

Based on the previous theoretical derivation, the evolution of radial velocity, local mass fraction and density are taken into account in the stead spray field. Considering the self-similarity of the velocity and fuel concentration fields, the following Gaussian radial profile can be considered in the developed spray region:

$$C = \frac{m_f}{m_a + m_f} \tag{18}$$

$$C(z,r) = C_{axis}(z)e^{-\alpha \cdot Sc \cdot \omega^2} \tag{19}$$

$$C_{axis}(z) = \frac{U_{axis}}{U_{exit}} \tag{20}$$

where $C(z,r)$ is the local fuel concentration, S_c is the Schmidt number, and according to the J.M. Desantes' conclusion[1], the S_c ranges from 0.6 to 1.4 and tiny effects on the axial velocity. In the current case, Sc=1.

According to the conclusion of Pickett [30], the radial profile given by Eq. (18) represents the fuel liquid volume fraction with no explicit consideration of fuel evaporation. In addition, the model assumes no velocity slip between injected fuel and entrained gases. Accordingly, momentum transfer between fuel droplets and entrained gas is assumed to be fully complete and the local fuel-ambient mixture is independent of whether there are droplets or vaporized fuel. Essentially, droplet size has no effect and there is no difference between this “spray” model and that of a hypothetical gas jet with the same momentum and mass flow rate. The local liquid volume fraction $\bar{\chi}(z,r)$ can be written as:

$$\bar{\chi}(z,r) = \frac{C(z,r)\rho_a}{(1-C(z,r))\rho_f + C(z,r)\rho_a} \tag{21}$$

Therefore, the model can be used to predict the local liquid volume fraction distribution within the spray. This simplified model is widely used as a tool to aid the interpretation of spray combustion measurements, including estimation of spray mixing to determine liquid-phase penetration length [19,23] or soot formation trends, as well as to guide spray models within more detailed CFD applications [28].

According to literature [23], a 1D spray model based on mixing-controlled hypotheses and the validity of self-similarity for conservation properties was established for the reaction conditions. The local spray density at an internal point of the spray, taking into account the local concentration, can be written for spray local concentration as follows:

$$\rho(z,r) = \frac{\rho_f \cdot \rho_a}{C(z,r)\cdot(\rho_a - \rho_f) + \rho_f} \tag{22}$$

3. Experimental spray measurement and Validation

3.1 Diffused back-illumination Imaging

The diffused back-illumination imaging technique illustrated in Fig.2 enables high-quality spray images. We adopted a double-pulsed Nd: YAG laser for illumination, which produces an original wavelength of 1064nm (infrared, invisible) as a fundamental beam, and then was frequency doubled under second harmonic generation to the wavelength of 532nm (green, visible). The green laser beam passes through the diverging lens, fluorescent class, milk diffusor and directly reaches the Constant Volume Spray Chamber (CVSC). A CCD camera with time intervals as small as 200 ns in the opposite direction was applied to capture the spray image shot-by-shot. The Davis system by Lavision was employed for the synchronization. A standard macro-lens (Nikon AF MICRO NIKKOR D150mm f/1:2.8) was attached to the camera. The final resolution was 2048×2048 and pixel resolution 40μm. In order to measure the fuel spray propagation, the images were captured by a 10μs interval from SOI (Start of Injection), and there were ten repetitions for each SOI.

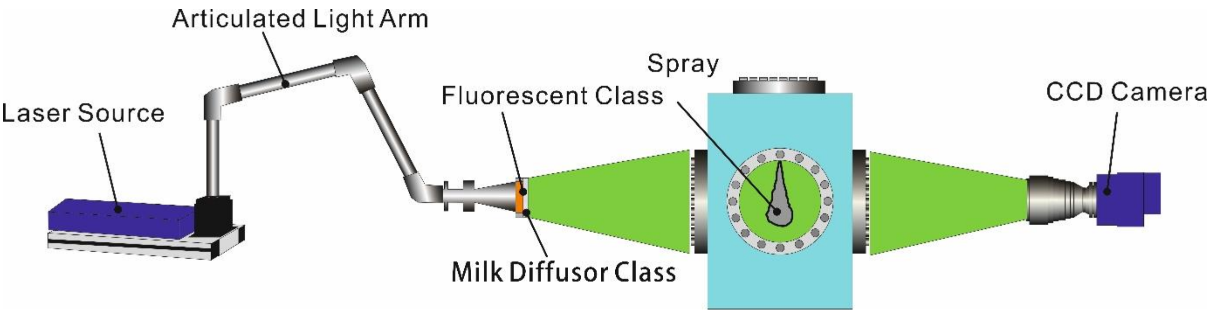

Fig.3 Diffused back-illumination imaging setup

3.2 Experimental Conditions and Fuel Properties

The measurements of fuel sprays were performed in a CVSC system under non-evaporative conditions at room temperature. The CVSC has four glass windows for light access, which located at four faces of the chamber. The diameter and the thickness of each window are 100mm and 30mm, respectively. A modern common rail fuel injection system based on Labview control system was performed to control the fuel pressure and injection timing. A solenoid-operated common rail injector form L'orange was employed for the fuel jet. More details of the experimental conditions are shown in Tab.1

Tab.1 Experimental conditions

Fuel Type	HVO,EN590
Ambient Density, (kg/m^3)	36,115
Ambient Temperature, (K)	293
Fuel temperature, (K)	293
Nozzle Dimeter, (mm)	0.12

Given the present conditions of renewable energy strategy in the European Commission and the previous studies in the Internal Combustion Engine Research Group of Aalto University, the recent research focuses on the comparison of renewable hydrotreated vegetable oil (HVO) and crude oil based EN 590 diesel fuel (EN590). The properties of these two type of fuels are listed in Tab.2 [31,32].

Tab.2 Fuel properties of HVO and EN590

	HVO	EN590
Density@15 ^{o}C(kg/mm3)	779.9	843.0
Kinematic viscosity @ 40 °C (mm2 /s)	3.087	3.208
Suface tension(mN/m)	28	29
Heating Value(mJ/kg)	44.1	43
Reid Vapor Pressure(kPa)	<0.1	<1

3.3 Image Post-Processing

The characteristics of diesel-like spray are represented in terms of four macroscopic parameters: spray tip penetration, spray cone angle, average spray tip velocity, and average fuel area and volume. Dedicated image post-processing algorithms have to be developed to quantify the macroscopic parameters as indicated in Eqs.(16) and (17).

Fig.4 illustrates the flowchart of the image post-processing. Considering the shot-to-shot variations, ten repetitions for each SOI were acquired by CCD camera. The average image of the 20 repetitions was obtained with the Matlab code. The background image without any spray was prepared for subtracting. After the subtraction from the average and the background, the image was rotated to horizontal direction to facilitate analysis. A binary image was converted by setting an appropriate threshold for a mask image. From each single spray image a binarization process results in a corresponding contour and a spray tip penetration. A statistical method is applied to derive the average spray boundary based on the probability map [33]. In current study, the average spray boundary is defined as the border of the region where the probability is equal to or higher than 50%. Then the outer edge of the spray can be detected, and the spray cone angle and spray tip penetration can be calculated. The local velocity, fuel concentration, liquid volume fraction and density distribution will be calculated pixel-by-pixel after the model validation.

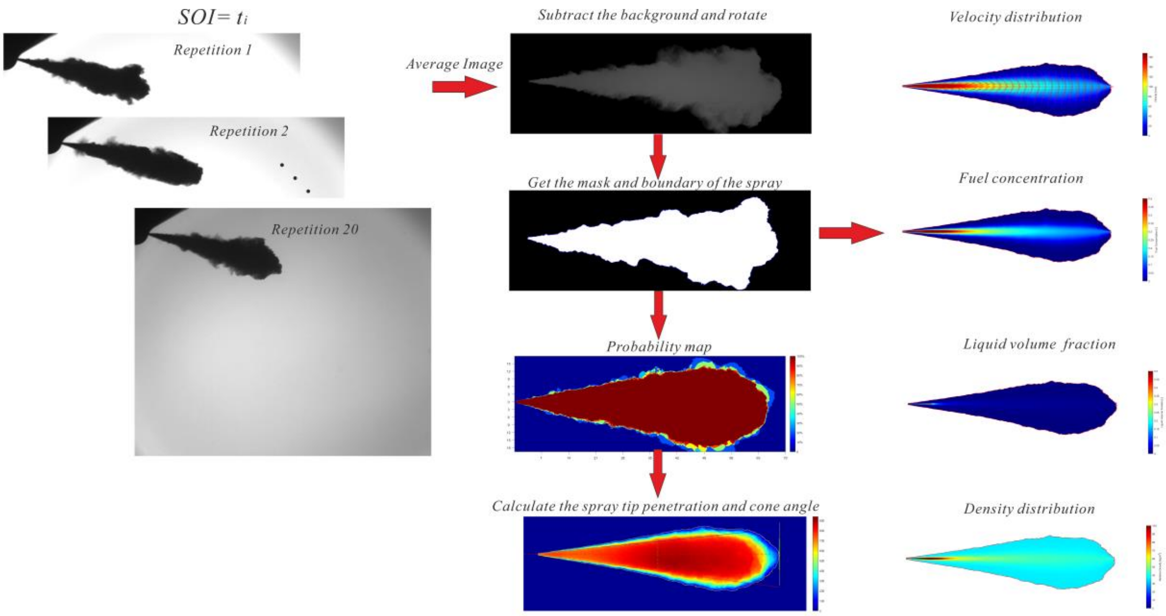

Fig.4 General overview of image post-processing

3.4 Theoretical Model Validation

To validate the theoretical model, the injection pressure, ambient density and fuel density were employed as inputs to the simulation model. The fuel temperature and ambient temperature were set at 293K, which assuming the fuel spray propagates under non-vaporized conditions.

According to the definition of the spray penetration and spray cone angle, these parameters can be obtained from the images directly [29]. Fig.5 shows the comparison of the experimental and modeling results. It can be discernible that the modeled results agree well with the experimental results.

It is worth noting that the variation caused by an increase in the ambient density can be accurately predicted without changing any input parameters. The penetration decreases with increasing ambient air density, due to higher resistance for the spray movement and more air entrainment into the spray. The high resistance of the ambient air reduces the flow velocity and leads to a shorter spray penetration. This effect can be derived from Eq. (16) directly. With increasing the ambient air density the higher obstruction for spray movement, which reduces on-axis variables and, consequently, spray velocity is lower [36]. There was no remarkable difference in spray penetration between the HVO and EN590, although the fuel density and viscosity of HVO is lower than EN590. These results are coincident with the conclusions in the literature [37]. According to the Eq.(16), the main factors influencing the spray tip penetration include ambient density, the momentum at the nozzle exit and spray cone angle. It is easy to conclude that, the ambient air density is the primary parameter influencing the spray tip penetration and spray cone angle, which can be derived from Eq.(17). Eq.(6) shows that the initial velocity at the nozzle exit was only influenced by the fuel pressure, ambient air pressure and fuel density. Owing to the small exponential factor in Eqs.(6) and (17), fuel density has a lower effect on spray tip penetration.

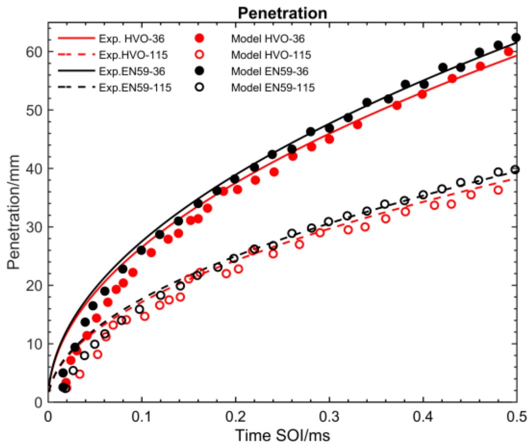

Fig.5 Comparison of experimental and modeled spray tip penetration under different ambient densities

The spray cone angle of HVO and EN590 at different ambient densities are illustrated in Fig.6. The stable spray cone angle from 0.1ms to 0.5ms ASOI was considered for comparison. Due to the spray variations, lead to the trends of spray cone angle is difficult to discern from experimental data. Therefore, the mean spray cone angle was compared with the experimental and modeled results. It is observed that higher ambient density results in a slightly larger spray cone angle. With higher ambient air density, these trends, caused by the increased resistance acting on a frontal area of the spray, leads to a greater momentum transfer between the spray and the ambient air, which increases the kinetic energy in the transverse direction. It can be observed that HVO has slightly bigger spray cone angle than EN590, these trends should be attributed to the Stokes number of the droplets, which is defined as the ratio of the characteristic time of a particle (or a droplet) to the characteristic time of the flow. In the case of the Stokes flow, the lower Reynolds number of the droplet results in higher drag coefficient[37]. Because the viscosity of the HVO is lower than the EN590, which occur in a higher Reynolds number, then leads to a smaller Stokes number. In addition, a lower Stokes number can cause instability between the fuel droplet and air entrainments. The vortex induced by the instability is expected to enhance the radial dispersion and result in a larger spray cone angle.

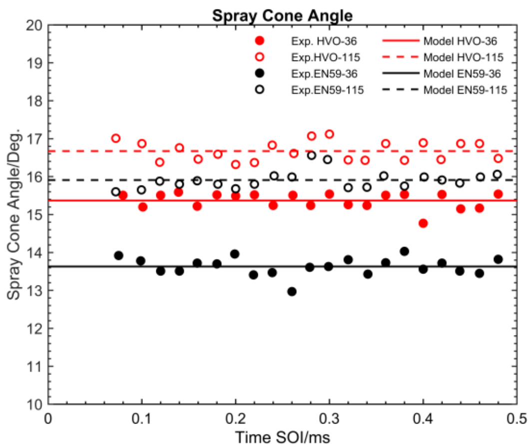

Fig.6 Comparison of experimental and modeled spray cone angle under different ambient densities

The comparison of the experimental and modeled axial velocity are shown in Fig.7. The modeled axial velocity is calculated from Eq. (13), in which the nozzle-exit velocity and spray cone angle are computed by means of Eqs.(6) and (17), respectively. The spray tip velocity can be obtained from image post-processing with different timing. Then the experimental axial velocity can be calculated by Eq.(15). It is noticeable that the axial velocity near the nozzle with the 1D model is over predict compared to the axial velocity with measurements. That might be attributed to the instability between the liquid phase and air entrainment. Because the atomization and mixing process is complicated in the near-nozzle field and the total momentum transfer assumption of the 1D model might not be appropriate. Moreover, the axial velocity in the near-nozzle field is close to the ambient air speed of sound which should be taken into account the model. However, after this first transient phase, the agreement between the model and the experimental data is acceptable. The axial velocity experiences an exponential decay because of the interaction between the liquid phase and ambient air. The higher ambient air density implies higher resistance for the fuel spray propagation and then leads to a lower axial velocity. The axial velocity of HVO is slightly smaller than the EN590 should be attributed to the lower density and viscosity which can be derived from Eq.(13) and Eq.(16).

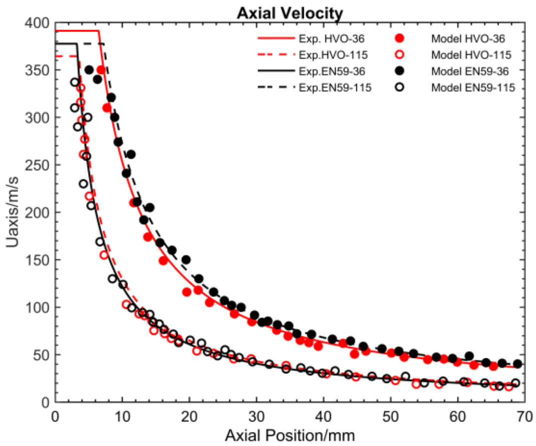

Fig.7 Comparison of experimental and modeled spray axial velocity under different ambient densities

The spray volume plays an important role in evaluating the quality of fuel–air mixing. It can be calculated through the following equation [38]:

$$V = \left(\frac{\pi}{3}\right) S_{tip}^{3} tan^{2}\left(\frac{\theta}{2}\right) \frac{1+2tan\left(\frac{\theta}{2}\right)}{\left[1+tan\left(\frac{\theta}{2}\right)\right]^{3}} \tag{23}$$

In the above fomula, S_{tip} is the spray tip penetration and θ is the spray cone angle.

The calculated spray volumes of HVO and EN590 under different ambient air densities are shown in Fig.8. Because the spray volume is the third power of S_{tip} and θ, the deviation might be magnified. Therefore, it is suitable to validate the accuracy of the model. The experimental spray volume is obtained from the image post-processing. Owing to the asymmetry structure of the real spray, the spray divided into two parts, above and below the spray axis. The spray volume of different parts is calculated independently and then divided into two to obtain the mean value. Fig.7 indicates that the spray volume at higher ambient air density is lower than the spray volume at lower ambient air density. This is because the spray propagation is restrained under the higher ambient air density, which results in lower spray tip penetration and slightly larger spray cone angle. However, the spray tip penetration has a stronger influence on spray volume than the spray cone angle. As a consequence, the longer spray tip penetration to lower ambient air density contributes more to spray volume than in higher ambient air density. Due to the slightly longer spray tip penetration of EN590, the spray volume of EN590 is marginally larger than the HVO because of the longer spray tip penetration.

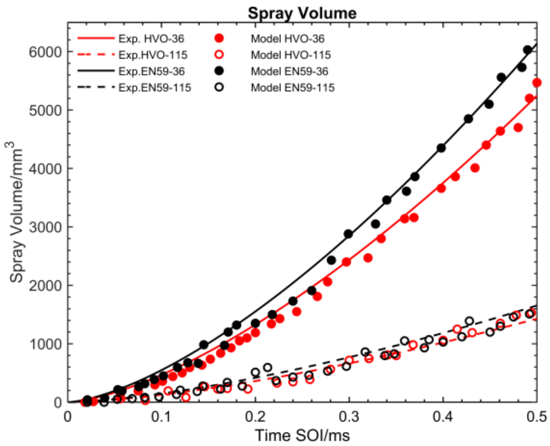

Fig.8 Comparison of experimental and modeled spray volume under different ambient density

4 Spray Radial Distribution

4.1 Velocity Distribution

According to Eqs.(13) and (14), the velocity in axial direction (U_{axis}) and in radial direction (U_{rad}) can be calculated pixel-by-pixel based on Gaussian radial profile and spray outer edge. Fig.9 shows the HVO and EN590 spray velocity distribution at 0.5ms ASOI under ambient air density 36kg/m^3 and 115kg/m^3. The red border is the outer edge of the spray, and the false-color images show the value of the resultant velocity (the velocity combined U_{axis} and U_{rad}). The red arrows represent the velocity distribution at axial direction. It can be observed that there is a distinct velocity decay at the downstream of the nozzle. The velocity near the nozzle exit is higher than the velocity at the spray tip and the velocity near the outer edge. It is worth noting that the velocity distribution is calculated based on the spray outer edge. Thus the velocity distribution is strongly correlated with the spray edge. It can be observed that there is no remarkable velocity difference between HVO and EN590 at lower ambient air densities. However, the velocity distribution of HVO and EN590 at higher ambient density seems more easily discernible due to the wrinkling of the outer edge.

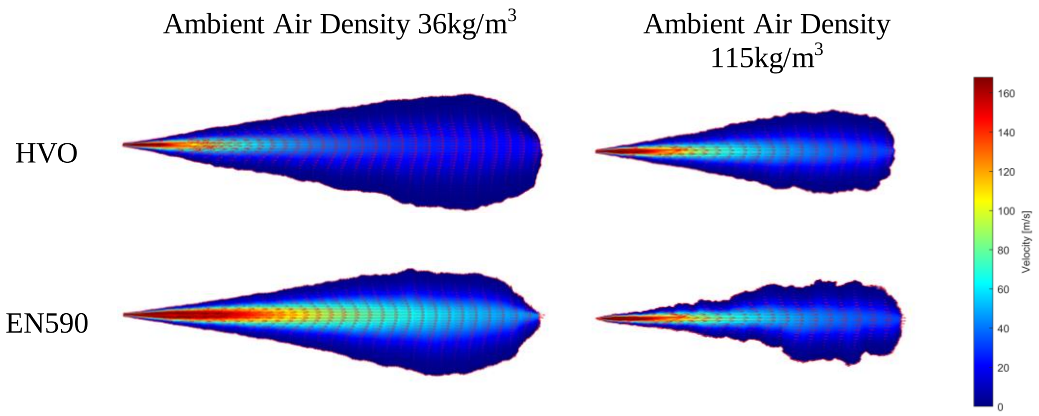

Fig.9 HVO and EN590 Spray velocity distribution at different ambient air densities

It should be noted that the Dis=10, 20, 30 and 40mm represent the distances of downstream of the nozzle exit at different fuel jet cross sections (10 mm, 20 mm, 30 mm,40mm). Fig.10 (a)-(d) illustrates the axial velocity of HVO and EN590 at the different Dis. It can be observed that the axial velocity of EN590 is slightly higher than HVO at the near-axis and near-nozzle zones. However, at the distantaxis, the axial velocity of EN590 is slightly lower than the HVO. It is notable that the spray width of HVO is slightly larger than EN590 at the same distance and the same ambient air density. This tendency means that the lower density and viscosity are causing the lower tip velocity and larger spray cone angle. This might be attributed to the air interaction on the low density and viscosity fuel. Similarly to the previous explanation, the low viscosity of fuel means higher Reynolds number, which results in higher sensitivity with the air entrainment. It is obviously found that the ambient air density has significant effects on the spray velocity. The axial velocity is decreased with the increase of the ambient air density. This can be explained by Eq.(13). The higher ambient air density results in higher resistance on the spray movement. An asymmetric curve of EN590 can be seen at Dis=40mm. This asymmetry is caused by the asymmetry of spray geometry near the tip.

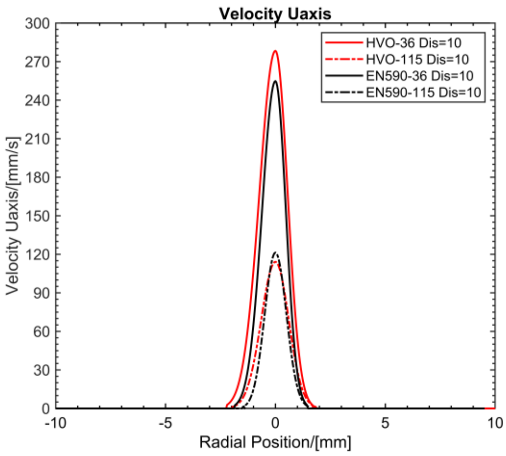

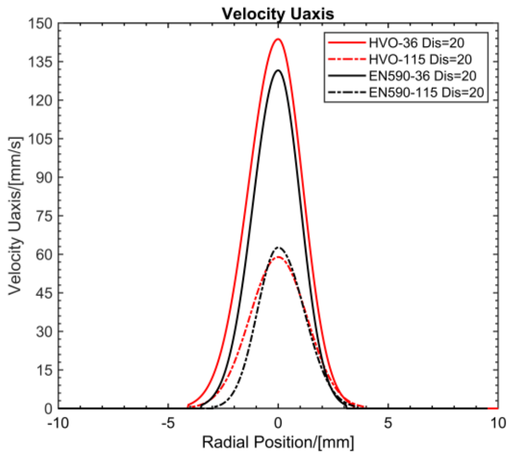

(a) Dis=10mm (b) Dis=20mm

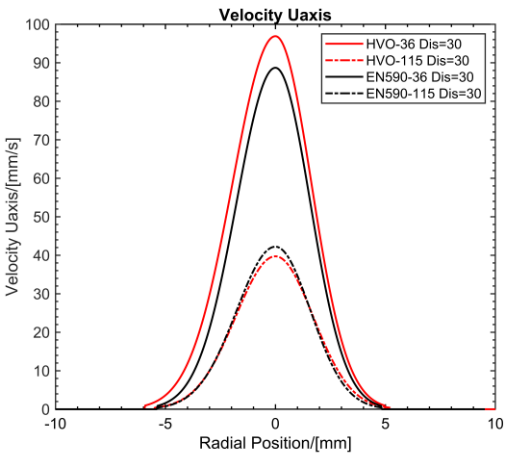

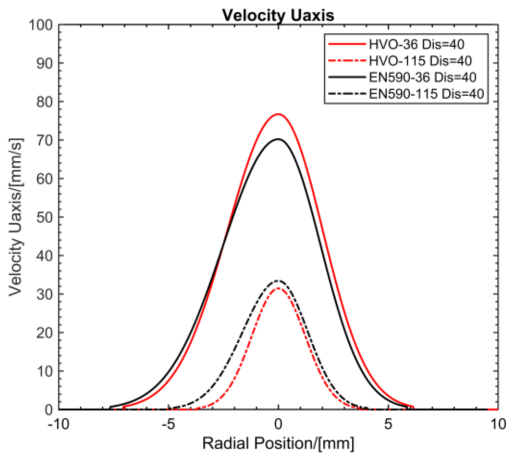

(c) Dis=30mm (d) Dis=40mm

Fig.10 HVO and EN590 axial velocity in radial direction at different downstream distances

The radial velocity at different axial distances provides additional insight into the spray propagations illustrated in Fig.11. It is notable that the radial velocity is completely incompatible with the axial velocity. There are two opposite directions for radial velocity, which correspond to the velocities at upper and lower side. It can be seen that there are two opposite peaks for radial velocity. However, In the center axis, the radial velocity in the center axis n is zero, which corresponds to no radial velocity component in the radial direction. This conclusion may not agree with the practical measurements, for instance, PIV or other optical approaches. Because the diesel-like spray is highly turbulent, the value and direction of the spray velocity are highly fluctuant. However, the simplified model for spray velocity in the radial direction can be used to estimate the average velocity distribution. It can be observed that there is a significant difference of radial velocity between the high and low ambient densities. Higher ambient air density results in higher resistance for the spray expansion in the radial direction. It is also notable that relatively higher radial velocity at low ambient air density occurs on HVO rather than EN590 due to the lower density and viscosity, which results in lower Stokes number and drag-coefficient of the droplets. However, at the higher ambient air density condition, the peak values of HVO and EN590 are almost the same. Hence, the radial velocity of the spray is insensitive to the fuel properties at high ambient air density conditions.

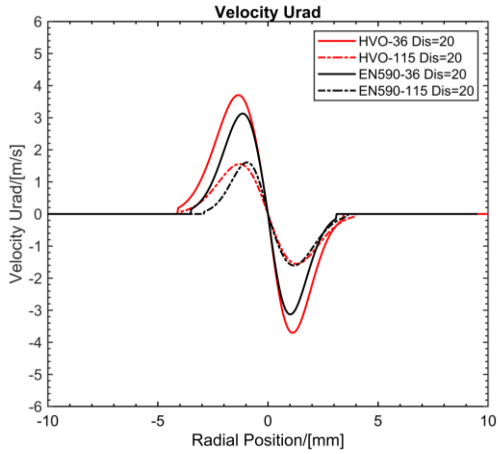

(a) Dis=10mm

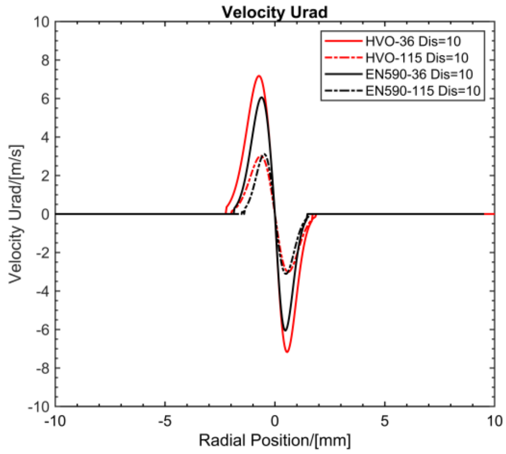

(b) Dis=20mm

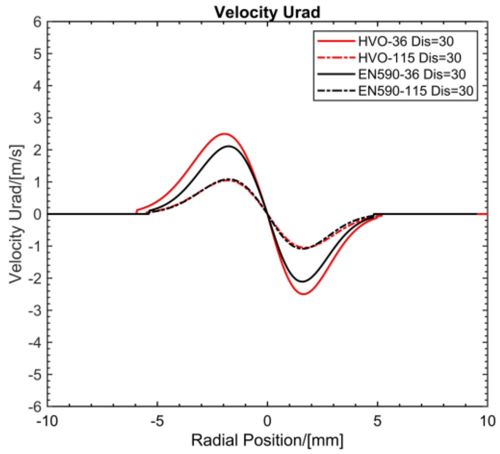

(c) Dis=30mm

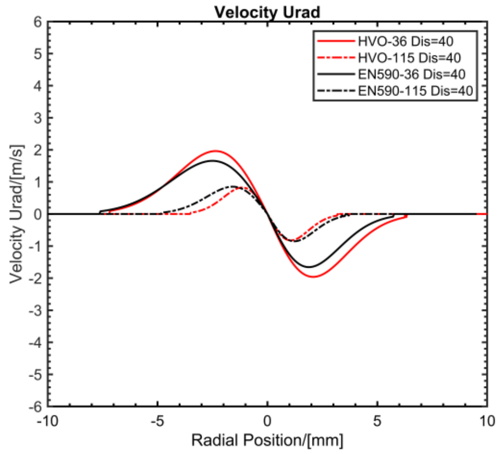

(d) Dis=40mm

Fig.11 HVO and EN590 radial velocity in radial direction at different downstream distances

4.2 Fuel Concentration Distribution

Fig.12 illustrates the fuel concentration of HVO and EN590 at 0.5ms ASOI under two ambient air densities at different fuel jet cross sections (10 mm, 20 mm, 30 mm,40mm). A significant gradient of fuel concentration in the spray can be discernible, both in axial and radial directions. The ratio of radial position and spray width ($\omega = r/R$) is adopted in this radial profile for the outer edge of the spray, where the modeled mixture fraction is zero. According to the conclusion in [30], the fuel spray has a smaller spreading angle in the near-field and transitions to a larger angle in the far-field. As a consequence, there is a smaller gradient of fuel concentration in the near-nozzle and a larger gradient of fuel concentration in the spray tip. As interpretation in Section 3.4, the local fuel concentration at a different position is determined by the model inputs, which include the fuel spreading angle, ambient air density, liquid fuel density and the spray edge based on the imaging. It is interesting to note that higher ambient air density leads to a larger gradient of fuel concentration. Meanwhile, higher liquid fuel density also leads to a larger gradient of fuel concentration. It can be concluded that the HVO has more optimal mixing characteristics than EN590 due to the relatively lower density.

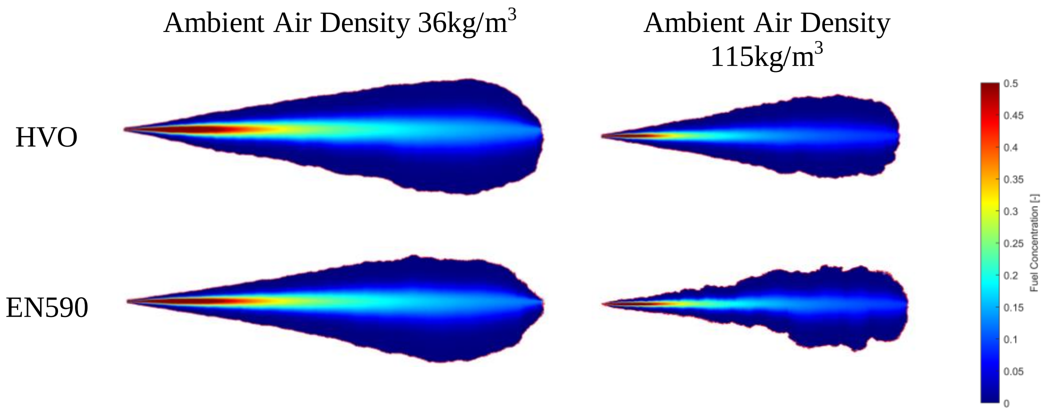

Fig.12 HVO and EN590 fuel concentration at the different downstream distance

Fig13(a-d) indicates the fuel concentration of HVO and EN590 under different ambient air densities at different fuel jet cross sections (10 mm, 20 mm, 30 mm,40mm). It is predicted that the radial fuel concentration profiles are self-similar, also self-similar within axial distance. Owing to the higher axial velocity U_{axis} of the EN590, which also represents higher fuel concentration in axial direction, this can be derived from Eq.(20). The radial profiles of the fuel concentration indicate that the gradient of fuel concentration at low ambient air density is larger than at the high ambient air density. This is because the high ambient air density obstructs the fuel propagation, although a similar amount of fuel is injected into the lower and higher ambient density environments, the spray volume in lower ambient air density is an order of magnitude larger than in the higher ambient air density. It can be observed that the shape of the fuel concentration profiles is similar to the axial velocity profiles in Fig. 10. The results are in agreement with the conclusions presented in [13].

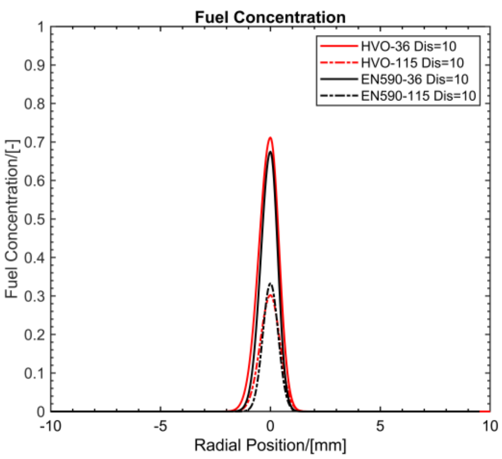

(a) Dis=10mm

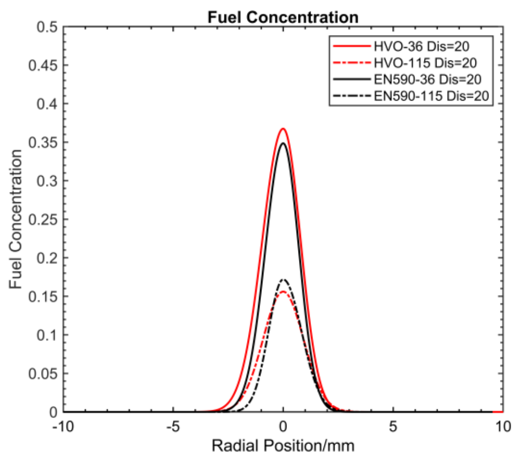

(b) Dis=20mm

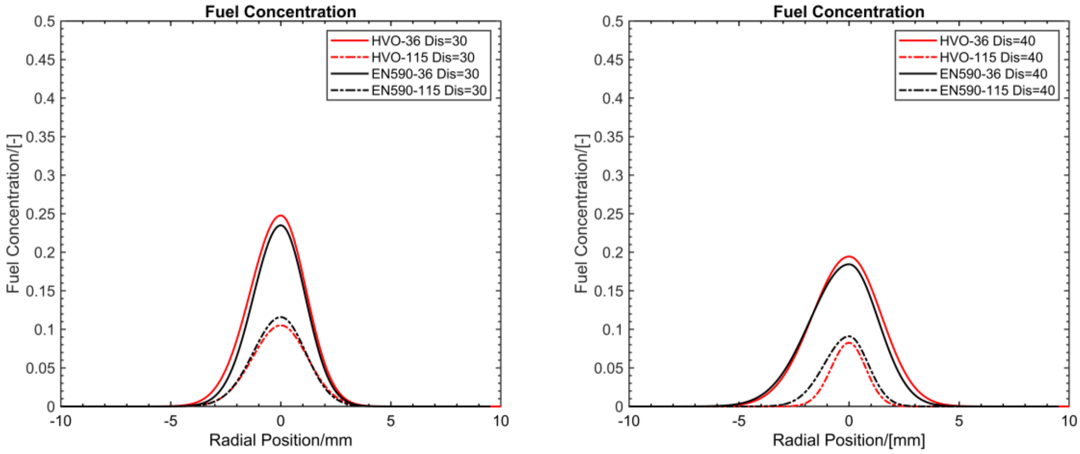

(c) Dis=30mm (d) Dis=40mm

Fig.13 Fuel concentration of HVO and EN590 in radial direction at different downstream distances

4.3 Liquid Volume Fraction Distribution

Fig.14 indicates the liquid volume fraction of HVO and EN590 at 0.5ms ASOI under two different ambient air densities, 36kg/m^3 and 115kg/m^3. It can be observed that the local liquid volume fraction has an extremely high gradient. It is related to the spray volume expansion and fuel concentration, which has been illustrated in Fig.7 and Fig.13. It is notable that the visible liquid volume fraction in the false-color images (Fig.14) only appear at the near-nozzle exit and close to the center axis. The interpretation of this phenomenon can be attributed to the spray volume expansion, because after the fuel jet is out from the nozzle, the liquid fuel experiences primary and secondary breakups and breaks into thousands of tiny droplets, meanwhile the spray volume is also thousands of times larger than initial stage due to the droplets movement and air entrainment. It is not difficult to observe that the ambient air density has dramatic effects on the liquid volume fraction. It can be seen that the length of the visible liquid volume fraction in the false-color images is less than half of the spray tip length at lower ambient density condition with HVO and EN590. However, this value is more than half of the spray tip length at higher ambient density condition. The interpretation is that the volume expansion rate at lower ambient air density is much higher than at the higher ambient air density due to less resistance for the spray movement. The reason can be interpreted in Fig. (7) and Eq. (21). No significant difference in liquid volume fraction is found in the false-color images between HVO and EN590 under the same conditions.

According to the definition of the liquid length in [40], the visible length of the liquid volume fraction can probably be used to estimate the spray liquid length under evarporating conditions, but the relationship is still remains unclear. However, it not difficult to conclude that the simplified liquid volume fraction model offers a highly accessible and straightforward method to quantify spray mixing.

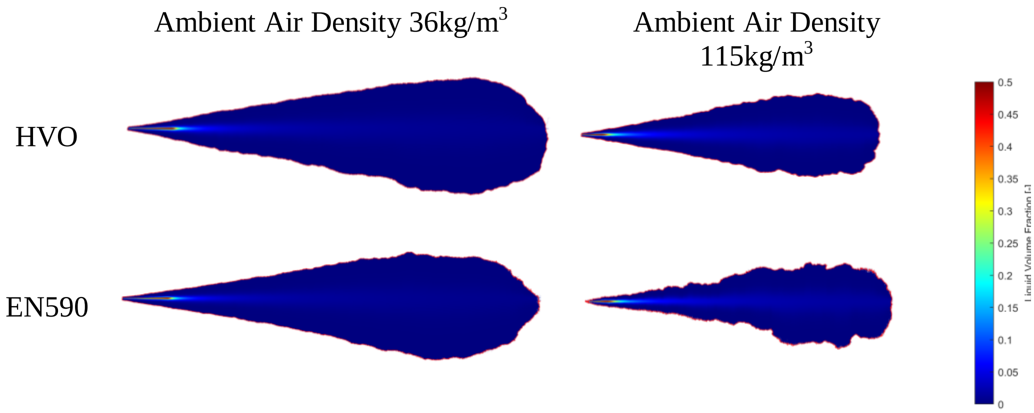

Fig.14 HVO and EN590 liquid volume fraction at different ambient air density

The local liquid volume fractions of HVO and EN590 under different densities at different fuel jet cross sections (10 mm, 20 mm, 30 mm, 40mm) are shown in Fig.15 (a)-(d). The fuel properties play a crucial role in liquid volume fraction near the nozzle exit zone, as can be observed in Fig.15 (a). However, with increasing distance, the influence of the fuel properties becomes weaker, which can be followed in Fig.15(b-c). This is because, at the initial stage, the entrainment mechanism is led by liquid phase, the liquid volume fraction is more dependent on the fuel properties, for instance, density and viscosity. However, at the far-end of the nozzle exit, the main entrainments are led by the ambient air, the liquid phase has fewer effects on the liquid volume fraction. It can be seen that the liquid volume fraction at the far-end (Dis=40mm) of the nozzle is small, and the maximum is only about 0.01. The shape of the liquid volume fraction has the similar distribution as the axial velocity and fuel concentration. As a consequence, if an increase or decrease in velocity is matched by an increase or decrease in ambient entrainment, a well-known result for fuel liquid volume fraction can be predicted. Although the liquid volume fraction model has not been validated in current studies, similar measurements from previous studies [36, 39] based on Rayleigh-scatter mixing measurements have concluded that the experimental and model liquid volume fraction profiles edge forward near-zero at a similar radial distance.

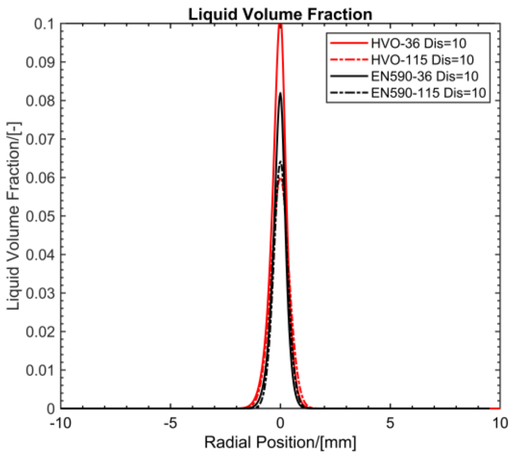

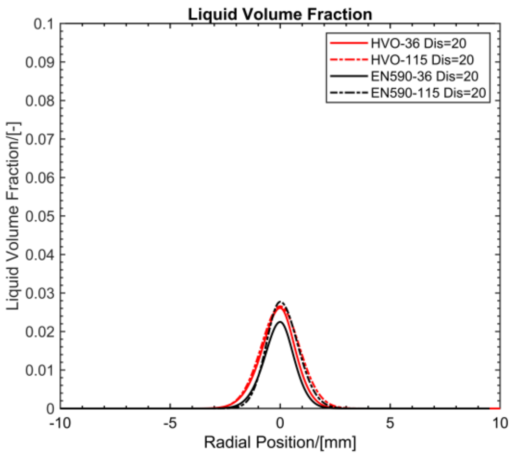

(a) Dis=10mm (b) Dis=20mm

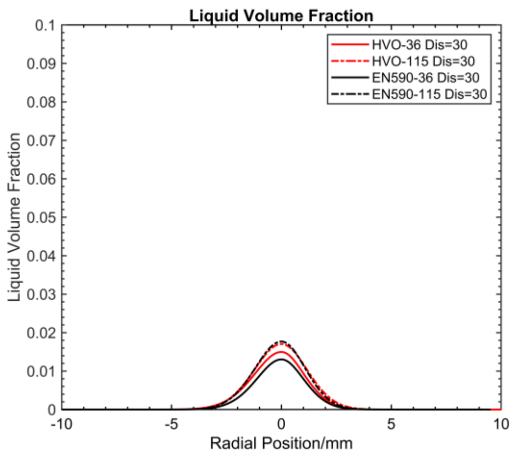

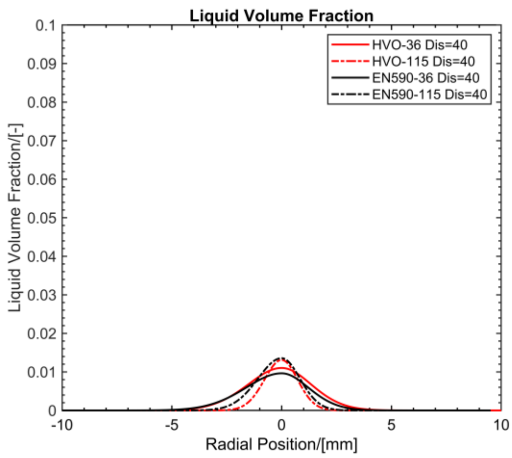

(c) Dis=30mm (d) Dis=40mm

Fig.15 HVO and EN590 liquid volume fraction in radial direction at different downstream distances

4.4 Spray density Distribution

Fig.16 shows the local spray density distributions of HVO and EN590 at 0.5ms ASOI under different ambient air densities. It is notable that the local spray density is the absolute density, which includes the ambient density. The spray density distribution has a high-density gradient from the nozzle exit to the tip. The spray near the nozzle exit and center axial has a higher density. However, the spray near the outer edge and the tip has a significantly lower density. This is because the spray density distribution substantially depends on the mass flow rate and spray volume. Once the liquid fuel jet is out from the nozzle, there is a great spray volume expansion. The spray volume expansion ratio can be derived from the Eq.(23). According to the analysis shown in Fig.7, the spray volumes of HVO and EN590 are close, and the mass flow rates of the HVO and EN590 are similar, which can be approximated with Bernoulli Function. Consequently, the spray density distributions of HVO and EN590 are similar under the same conditions. Because the spray density distribution is derived from the outer edge of the spray, as a consequence, the spray density distribution is highly dependent on the spray configuration. It implies that the similar spray geometry contains identical spray density gradient information under the same ambient air density.

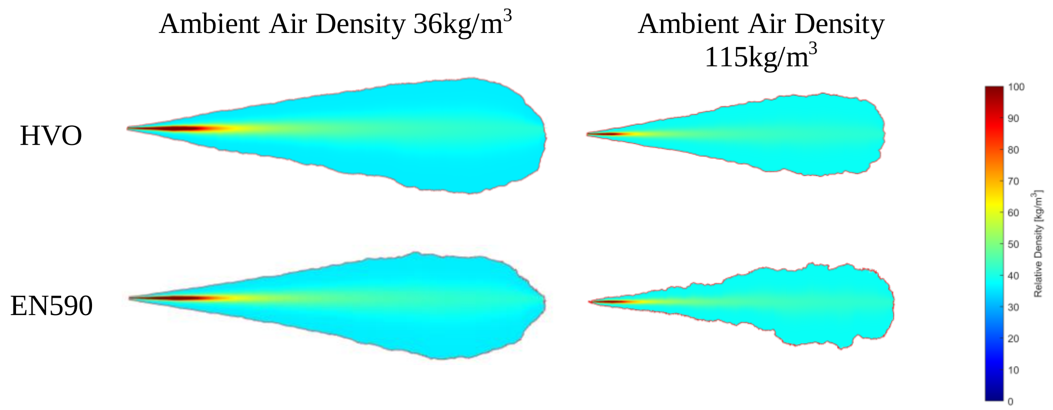

Fig.16 HVO and EN590 spray density distribution at different ambient air densities

To improve the comparability of the spray density at different positions downstream of the nozzle exit. The relative density was defined as the spray density subtract the ambient air density. The relative density of the HVO and EN590 at different positions of downstream the nozzle exit can be observed in Fig.17 (a)-(d). It is shown that the spray density at the higher ambient air density represents faster density decay than at lower ambient air density. At Dis=10mm, the spray density of HVO and EN590 at higher ambient air density is much higher than their spray density at lower ambient air density. However, at Dis=20mm, the spray density at lower ambient air density is slightly higher than the spray density at higher ambient air density, clearly exceeding the spray density at higher ambient air density at Dis=30 and 40mm. The spray density of EN590 is higher than the HVO in certain areas where near the axis center; however, because of the larger radius of the outer edge, the HVO has a broader spray distribution at Dis=10 and 20mm. However, at Dis=30 and 40mm, because of the effects of ambient air entrainments, the spray density distribution of HVO narrower than EN590.

Based on the X-Ray Radiography measurement on different nozzle geometry, a Gaussian curve fits the data more accurately at most measurement positions[39]. The distribution in local spray density distribution can be examined to quantify the behavior of the spray better.

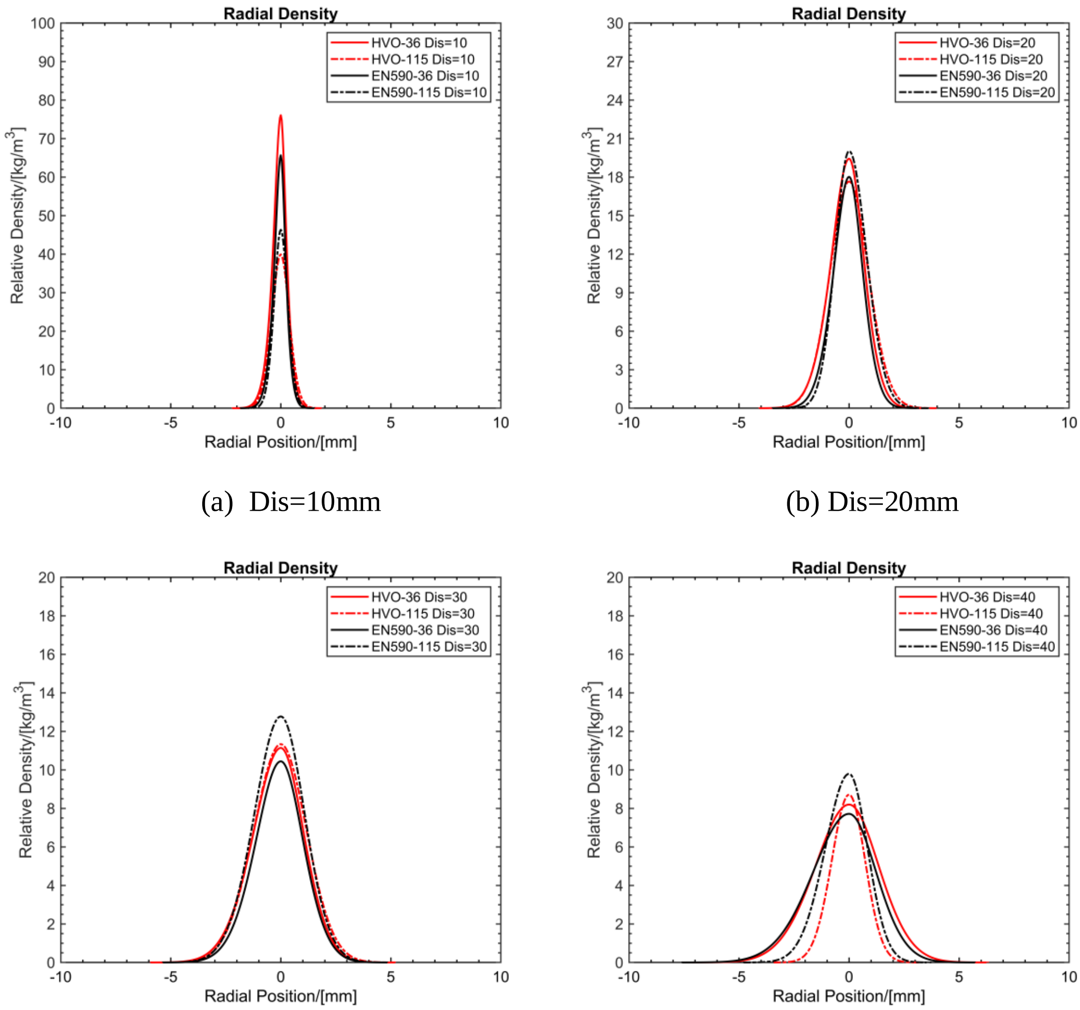

(a) Dis=10mm (b) Dis=20mm

(c) Dis=30mm (d) Dis=40mm

Fig.17 HVO and EN590 spray density in radial direction at the different downstream distance

5. Summary and Conclusion

This study aimed at understanding the behavior of diesel-like spray dynamics. For that purpose, the diffused back-illumination imaging technique was adopted to capture the spray images at different ASOIs. A 1D model based on physical considerations and empirical evidence was developed to predict the diesel-like spray characteristics. The major conclusions in this study are as follows:

(1) The theoretical model based on momentum flux in the axial direction was solved in terms of on-axis variables by assuming self-similar radial profiles for axial velocity and local fuel concentration. The input parameter such as velocity at the nozzle exit and spray cone angle were calculated and validated based on an empirical model. The diffused back-illumination imaging was performed to validate the accuracy of the model. The results show that the modeled results are in good agreement with the experimental results on spray tip penetration, spray cone angle, axial velocity, and spray volume. This encourages further consideration of axial and radial velocity, local fuel concentration, liquid volume fraction, and local density based on the Gaussian radial profile.

(2) The experimental arrangement based on diffused back-illumination was performed to measure the global spray characteristics of HVO and EN590 under different ambient air densities. According to the comparison, there were no remarkable differences in the spray geometry between the HVO and EN590.

However, the ambient air density seems to have notable effects on the spray dynamics, which can be explained by the momentum flux conservation.

(3)The quantitative comparison of spray characterisitcs of HVO and EN590 has been performed with experimental and modelled approaches. The differences of penetration, spray angle, axial velocity and spray volume are -1.96%, 13.08%, 3.17%, and -13.3% respectively at low ambient air density condition. At high air density condition, the differences are even smaller. The characteristics of local velocity, fuel concentration, liquid volume fraction and density distribution of HVO and EN590 are similar, which indicate that HVO appears to have the similar air-fuel premixing process compared to the conventional petroldiesel.

(4) In summary, the main contribution of the current investigation is the integration of momentum flux conservation, Gaussian radial profile to the practical image outer edge. This enables the visualization of the spray characteristics based on very straightforward optical measurements, other than complex diagnostics techniques such as PIV, PLIF or X-ray imaging.

Acknowledgments

The financial support from Aalto University, School of Engineering (Department of Mechanical Engineering) and Finnish Academy project (Grant No. 297248) are acknowledged.

6 References

[1] J.M. Desantes, R. Payri, J.M. Garcia, F.J. Salvador. A contribution to the understanding of isothermal diesel spray dynamics. Fuel 86 (2007) 1093–1101.

[2] Hiroyasu H, Arai M. Structures of fuel sprays in diesel engines, SAE Paper 900475, 1990.

[3] ZhijunWu, ZhiyongZhu, ZhenHuang. An experimental study on the spray structure of oxygenated fuel using laser-based visualization and particle image velocimetry. Fuel 85 (2006): 1458-1464

[4] Todd D. Fansler, Scott E. Parrish. Spray measurement technology: a review. Meas. Sci. Technol. 26 (2015) 012002:1-34.

[5] Fansler T D, Drake M C, Gajdeczko B, Düwel I, Koban W, Zimmermann F P and Schulz C 2009 Quantitative liquid and vapor distribution measurements in evaporating fuel sprays using laser induced exciplex fluorescence Meas. Sci. Technol. 20 125401

[6] Junyong Lee, Namho Kim and Kyoungdoug Min. Measurement of spray characteristics using the background-oriented schlieren technique. Meas. Sci. Technol.24(2013) 025303 : (1-9).

[7] Launder BE, Spalding DB. Mathematical models of turbulence. Academic Press; 1972.

[8] Alfonsi G. Reynolds-Averaged Navier–Stokes Equations for Turbulence Modeling. ASME. Appl. Mech. Rev. 2009, 62(4):040802-040802-20.

[9] Simin Anvari, Hadi Taghavifar, Shahram Khalilarya, et al. Numerical simulation of diesel injector nozzle flow and in-cylinder spray evolution [J]. Applied Mathematical Modelling. 2016, 40(19–20): 8617-8629.

[10] Noah Van Dam and Christopher Rutland. Adapting diesel large-eddy simulation spray models for direct-injection spark-ignition applications. International Journal of Engine Research. 2015, 17(3): 291-315

[11] Orszag, Steven A. Analytical Theories of Turbulence. Journal of Fluid Mechanics. 41 (1970): 363–386

[12] Masataka Arai. Physics behind Diesel Sprays [C]. ICLASS 2012, 12th Triennial International Conference on Liquid Atomization and Spray Systems, Heidelberg, Germany, September 2-6, 2012.

[13] J.M. Desantes, R. Payri , J.M. Garcia, F.J. Salvador. A contribution to the understanding of isothermal diesel spray dynamics. Fuel 86 (2007):1093-1101

[14]Payri F, Bermu´dez V, Payri R, Salvador FJ. The influence of cavitation on the internal flow and the Spray characteristics in diesel injection nozzles. Fuel 83(2004): 419-31.

[15] J.M. Desantes, R. Payri, F.J. Salvador, A. Gil. Development and validation of a theoretical model for diesel spray penetration. Fuel 85 (2006):910-917.

[16] R. Payri, F.J. Salvador, J. De la Morena, V. Pagano. Using a one-dimensional spray model to improve liquid length and ignition delay estimations for diesel flames. Applied Thermal Engineering 124 (2017):1090-1102.

[18]Ueki H., Ishida D., Naganuma M.. Simultaneous Measurements of Velocity and size of diesel fuel near nozzle orifice by Laser 2-Focus velocimeter with Micro-Scale Porbe volume THIESEL 2004 Conference on Thermo-and fluid Dynamic Processes in Diesel Engines 2004.

[19] Dennis L. Siebers. Scaling Liquid-Phase Fuel Penetration in Diesel Sprays Based on Mixing-Limited Vaporization. SAE Trans. 1999, 108(3):703-728.

[20] Desantes JM, Arre`gle J, Lo´pez JJ, et al. Scaling laws for free turbulent gas jets and Diesel-like sprays. Atomization and Spray 16(2006b): 443-473.

[21] Hinze JO. Turbulence. McGraw Hill, New York,1975.

[22] Sinnamon JF, Lancaster DR, Stiener JC (1980) An experimental and analytical study of engine fuel spray trajectories. SAE Paper 800135

[23] J.M. Desantes, J.V. Pastor, J.M. García-Oliver, J.M. Pastor. A 1D model for the description of mixing-controlled reacting diesel sprays. Combustion and Flame 156 (2009): 234-249

[24] Christopher von Kuensberg Sarre, Song-Charng Kong, and Rolf D. Reitz. Modeling the effects of injector nozzle Geometry on Diesel Spray [J]. SAE PAPER, 1999, 1999-01-0912.

[25] Benedict, R.P. Fundamentals of Pipe Flow [M], Wiley, New York,1980.

[26] Nurick WH. Orifice cavitation and its effect on spray mixing. J Fluids Eng 98(1976):681–7.

[27] Lionel Martinez, Adlène Benkenida, Bénédicte Cuenot. A model for the injection outer edge conditions in the context of 3D simulation of Diesel Spray: Methodology and validation. Fuel 89 (2010): 219-228.

[28] J.M. García-Oliver, X. Margota, M. Chávez, et al. A combined 1D3D–CFD approach for reducing mesh dependency in Diesel spray calculations. Mathematical and Computer Modelling 54 (2011): 1732-1737.

[29] Reitz RD, Bracco FV. Mechanisms of breakup of round liquid jets. Encyclopedia Fluid Mech 1986: 233-249.

[30] Pickett, L., Manin, J., Genzale, C., Siebers, D. et al., "Relationship Between Diesel Fuel Spray Vapor Penetration/Dispersion and Local Fuel Mixture Fraction," SAE Int. J. Engines 2011, 4(1):764-799.

[31]Aatola, H. Larmi, M. Sarjovaara, T. Mikkonen, S. Hydrotreated Vegetable Oil (HVO) as a Renewable Diesel Fuel: Trade-off between NOx, Particulate Emission, and Fuel Consumption of a Heavy Duty Engine. SAE Technical Paper 2008, 2008-01-2500.

[32] Tilli, A., Imperato, M., Aakko-Saksa, P. Larmi, M., Sarjovaara, T., Honkanen M. High Cetane Number Paraffinic Diesel Fuels and Emission Reduction in Engine Combustion. CIMAC Paper 26, 2010.

[33] Payri R, García JM, Tiemin Xuan, et al., A study on diesel spray tip penetration and radial expansion under reacting conditions. Appl.Therm.Eng.2015; 90: 619-629.

[34] Payri R, Garcı´a JM, Salvador FJ, Gimeno J (2005) Using spray momentum flux measurements to understand the influence of diesel nozzle geometry on spray characteristics. Fuel 84(2005):551-561

[35] F. Payri, R. Payri, M. Bardi,M. Carreres. Engine combustion network: Influence of the gas properties on the spray penetration and spreading angle. Experimental Thermal and Fluid Science 53(2014):236-243.

[36]J. Kostas, D. Honnery, J. Soria, et al.Effect of nozzle transients and compressibility on the penetration of fuel sprays. Appl. Phys. Lett., 95 (2009) 024101-1:3.

[37] José V. Pastor, J. Javier López, José M. García, et al. A 1D model for the description of mixing-controlled inert diesel sprays. Fuel 87 (2008) 2871–2885.

[38] Vuorinen Ville, Hillamo Harri, Kaario, Ossi, et al. Large-Eddy Simulation of Droplet Stokes Number Effects on Turbulent Spray Shape. Atomization and Sprays, 2010, 2(20): 93-114.

[39] E. Delacourta, B. Desmeta, B. Besson. Characterisation of very high pressure diesel sprays using digital imaging techniques. Fuel 84 (2005) 859–867.

[40] A. L. Kastengren, C. F. Powell, T. Riedel, et al. Nozzle Geometry and Injection Duration Effects on Diesel Sprays Measured by X-Ray Radiography. Journal of Fluids Engineering, 30(2008) 041301-1:12.

[41] Sanghoon Kook, Lyle M.Pickett. Liquid length and vapor penetration of conventional, Fischer–Tropsch, coal-derived, and surrogate fuel sprays at high-temperature and high-pressure ambient conditions. Fuel 93(2012): 539-548.